

See discussions, stats, and author profiles for this publication at: <https://www.researchgate.net/publication/226272041>

# A Geochemical study of the groundwater in the Misli basin and environmental implications

Article *in* Environmental Geology · January 2007

DOI: 10.1007/s00254-006-0460-5

---

CITATIONS

14

---

READS

24

1 author:



Galip Yuce

Hacettepe University

55 PUBLICATIONS 150 CITATIONS

SEE PROFILE

# A Geochemical study of the groundwater in the Misli basin and environmental implications

Galip Yuce

Received: 11 March 2006 / Accepted: 7 August 2006 / Published online: 8 November 2006  
© Springer-Verlag 2006

**Abstract** The aim of this study was to determine geochemical properties of groundwater and thermal water in the Misli Basin and to assess thermal water intrusion into shallow groundwater due to over-extraction. According to isotope and hydrochemical analyses results, sampled waters can be divided into three groups: cold, thermal, and mixed waters. Only a few waters reach water–rock chemical equilibrium. Thermal waters in the area are characterized by  $\text{Na}^+ - \text{Cl}^- - \text{HCO}_3^-$ , while the cold waters by  $\text{CaHCO}_3$  facies. On the basis of isotope results, thermal waters in the Misli basin are meteoric origin. In particular,  $\delta^{18}\text{O}$  and  $\delta^2\text{H}$  values of shallow groundwater vary from  $-10.2$  to  $-12.2\text{‰}$  and  $-71.2$  to  $-82\text{‰}$ , while those of thermal waters range from  $-7.8$  to  $-10.1\text{‰}$  and from  $-67$  to  $-74\text{‰}$ , respectively. The tritium values of shallow groundwater having short circulation as young waters coming from wells that range from 30 to 70 m in depth vary from 10 to 14 TU. The average tritium activity of groundwater in depths more than 100 m is  $1.59 \pm 1.16$ , which indicates long circulation. The rapid infiltration of the precipitation, the recycling of the evaporated irrigation water, the influence of thermal fluids and the heterogeneity of the aquifer make it difficult to determine groundwater quality changes in the Misli Basin. Obtained results show that further lowering of the groundwater table by over-consumption will cause further intrusion of thermal water which resulted in

high mineral content into the fresh groundwater aquifer. Because of this phenomenon, the concentrations of some chemical components which impairs water quality in terms of irrigation purposes in shallow groundwaters, such as  $\text{Na}^+$ , B, and  $\text{Cl}^-$ , are highly probably expected to increase in time.

**Keywords** Turkey · Misli basin · Groundwater · Thermal water · Hydrochemistry ·  $\delta^{18}\text{O}$  ·  $\delta^2\text{H}$  · Tritium

## Introduction

The Misli basin is located at about 35 km north of Nigde city in Central Anatolia (Fig. 1a). The area is approximately 1,325 km<sup>2</sup>. It is surrounded by the volcanoes such as the Melendiz, Erciyes, and Hasan Mountains (Fig. 1a). The continental climate conditions prevailed in the region, with hot and dry summers, and cold and rainy winters. The maximum temperature varies from 34 to 36°C in summers and the minimum temperature is  $-18^\circ\text{C}$  in winters. The mean elevation of the basin is 1,300 m and the mean annual precipitation is 347.2 mm.

Surface water in the basin flows intermittently due to the high permeability of alluvium which mainly consists of coarse volcanic debris. The Agacli spring is the only water source in the basin discharging from basalts (Fig. 1a). The maximum and minimum discharges of the spring were observed in 1970–1997 period are 4,740 l/s (May 1974) and 913 l/s (July 1980), respectively (Bursali et al. 1975). Governmental organizations and farmers drilled numerous wells in the area for irrigation and domestic purposes, and the

G. Yuce (✉)  
Department of Geological Engineering,  
Faculty of Engineering and Architecture,  
Eskişehir Osmangazi University,  
26040 Eskişehir, Turkey  
e-mail: gyuce@ogu.edu.tr

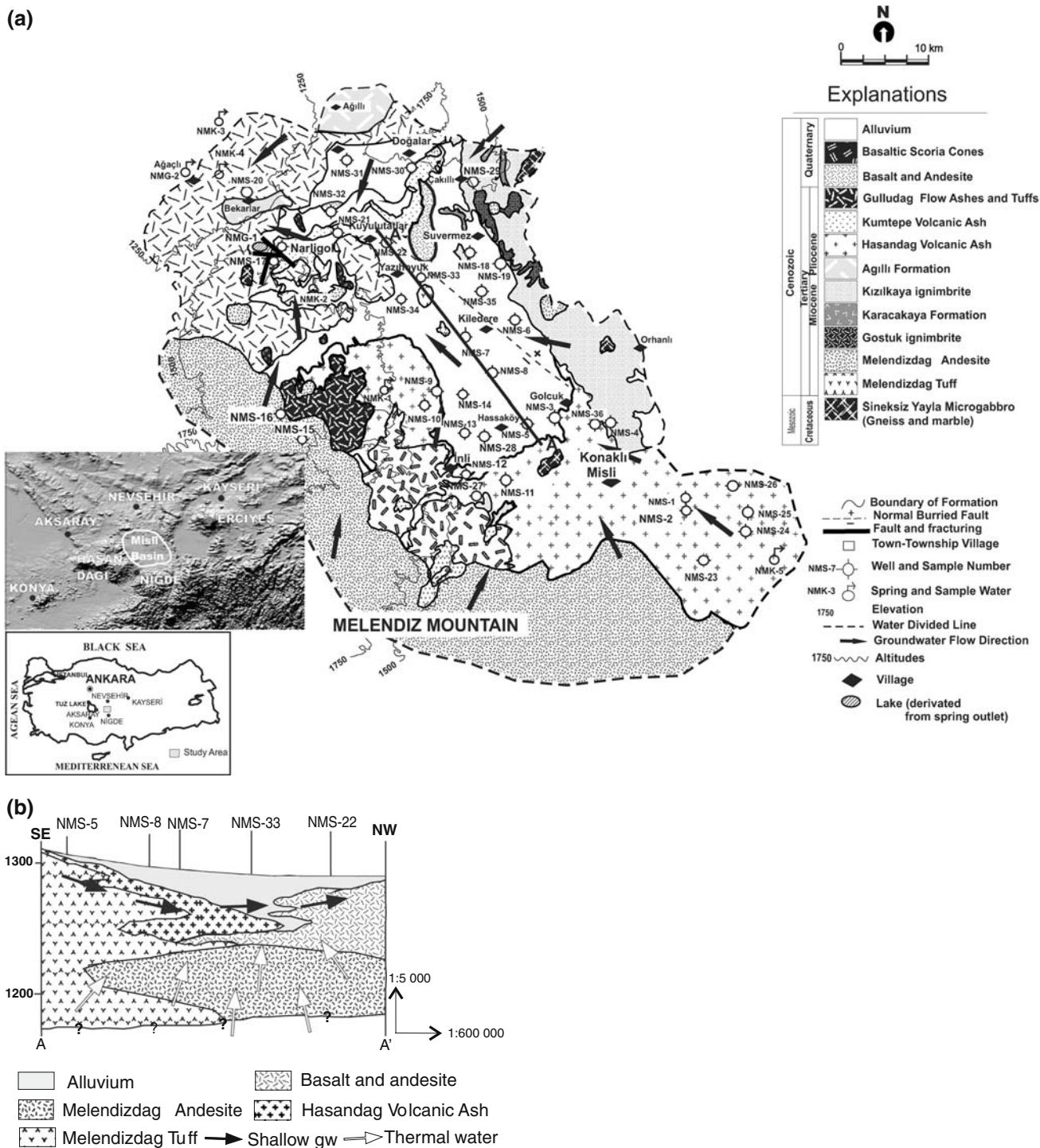


**Fig. 1** a Simplified geological–hydrogeological map of the study area (modified from Yurdagul 1998) and location of sampling points. b A geological cross-section of the study area

number of wells has increased in time. The depth of the wells ranges from 30 to 250 m and yield of them varies from a few liters to 60 l/s.

The first hydrogeological study in the area was conducted by Gulenbay (1971) and he calculated a safe annual yield of groundwater as 56 hm<sup>3</sup>. Later,

Yurdagul (1998) proposed a safe annual yield of groundwater as 115 hm<sup>3</sup>. According to his calculation, the annual groundwater recharge was approximately 135 hm<sup>3</sup>, whereas its annual groundwater extraction was 177.5 hm<sup>3</sup>, 147.5 hm<sup>3</sup> from wells and 30 hm<sup>3</sup> from the springs. Thus, the annual deficit of groundwater

mining was almost 42 hm<sup>3</sup> because of over-drawn from the reservoir. Therefore, this situation causes a drawdown by 2 m per year (Yurdagul 1998). In addition to this undesirable decreasing in groundwater level, the deeper part of the aquifer hosted by high-mineralized thermal water enriched in Na<sup>+</sup>–Cl<sup>–</sup>–HCO<sub>3</sub><sup>–</sup> by diffusive encroachment which deteriorates shallow groundwater quality for irrigation and domestic supplies.

## Methodology

Major ion analyses were performed as well as oxygen and hydrogen isotopes analyses in order to determine water composition of both thermal and shallow groundwater. Forty-six water samples were collected from the area. Two sampling campaigns were realized, in July and October 1998. The locations of water samples are given in Fig. 1a. Waters were sampled into polyethylene bottles after pumping the sampled in order to obtain freshwater. Water temperature, pH, and electrical conductivity (EC) were measured in situ using a Schott-Gerate handy lab model instrument with an accuracy of ±1 µS/cm for EC and sensitivity of ±0.01 for pH. Water samples for cation analysis were filtered 0.45 µm in the field and acidified with HNO<sub>3</sub> by 65% to stabilized ionization pH up to smaller than 2.0. Volumetric methods were used for determination of Ca<sup>2+</sup>, Mg<sup>2+</sup>, and HCO<sub>3</sub><sup>–</sup>. SO<sub>4</sub><sup>2–</sup> and Cl<sup>–</sup> were analyzed by ion chromatography. Na<sup>+</sup> and K<sup>+</sup> concentrations were determined by flame photometry. The samples for deuterium and oxygen-18 were not treated in the field and isotopes were determined by mass spectrometry in the laboratories of the Technical Research and Quality Control Department of DSI (State Hydraulic Works) in Ankara. Deuterium and oxygen-18 contents analyses have an overall precision of 1 and 0.1‰, respectively. These values are expressed in delta notation as per mil deviation from the Vienna Standard Mean Ocean Water (V-SMOW; Verhagen et al. 1991). Tritium was also analyzed in the same laboratory by a liquid scintillation counter (LSC) after electrolytic enrichment. The precision of this determination was ±0.8 TU for each sample.

## Geological and hydrogeological settings

The general geology and a geological cross-section of the study area is given in Fig. 1a and b. As can be seen from the map, volcanic rock outcrops widely covers the area. The basement rock which crops out in a very

limited area comprises of micro-gabbros of Cretaceous age. Volcanic activity began in Late Miocene and continued until the Quaternary, concentrating first around the Melendiz Mountain and later in the surroundings of the Hasan Mountain. The Miocene volcanic products of Melendiz Mountain consist of andesitic lavas, tuff, and ignimbrites. The volcanic products as well as volcano-sedimentary rocks such as sandstone, claystone, and breccias also crop out in the area. Basaltic scoria cones of Quaternary age are observed in the north of the basin. Quaternary alluvium and talus deposits consisting mostly of sand and gravel of igneous and volcanic origin are the youngest units in the area. Quaternary deposits and scoriaceous lavas (with high permeability) comprise the aquifer units.

During the Late Miocene, groundwater in the Misli Basin was probably discharging to the west. Both the faulting occurred along Kiledere and Suvermez, and the following sedimentation caused increase of the sediment thickness at footwall side of the fault. Continuous volcanic activity represented by basaltic flows and detrital sedimentation within different periods caused the rising of the basin elevation, and an impermeable level was formed because of this basaltic lava flow at the basement, and then these basalt eruptions started to close the western edge of the basin. Thus, groundwater was partially trapped in the middle part of the Misli Basin.

From the geological point of view, the Golcuk part of the basin consists of tuff, gravel, sand, and silt, and it comprises an unconfined aquifer while the Kiledere area comprises a confined aquifer due to the different levels of clay beddings (aquiclude). The aquifer is recharged directly by the precipitation from higher altitudes in the west and south of the basin, and some small springs occur in the nearby region. The Agacli spring (~1 m<sup>3</sup>/s), the biggest outflow of the area, has a low discharge in the dry season (in November and December) and a high flow rate in the wet season (in April and May), naturally. The recession coefficient of the spring was calculated as  $5.43 \times 10^{-4}$ /day and the annual discharge was 30 hm<sup>3</sup> according to runoff records from 1995 to 1997 (Yurdagul et al. 1998). Based on the water-level time-series data (from 1987 to 1997) of the wells, groundwater level decreased to 8–10 m. due to over-extraction. The general flow direction of groundwater in the area is from SE to NW–W where the Agacli spring manifestation (Fig. 1a). On the basis of pumping tests, the transmissivity coefficients of the aquifer were calculated in the ranges from 300 to 9,000 m<sup>3</sup>/day/m and storage coefficients were found varies from 0.15 to 0.25 for the unconfined aquifer (Yurdagul et al. 1998) in the area.

## Results and discussion

### Water chemistry

The ion concentrations of water samples are shown as pie diagrams on the map (Fig. 2). The water samples collected from wells (NMS-4, NMS-15, NMS-16, NMS-23, NMS-25, and NMS-36) represent  $\text{CaHCO}_3$  facies, and most of the shallow waters are mainly in Ca, Mg, and  $\text{HCO}_3$  facies. Probably, the ferromagnesian volcanic material in the central part of the basin causes a slight increase in the Mg content of groundwater.

Thermal waters are mainly observed in south and northwest of the basin around the village of Inli (NMS-11) and Narligol (NMS-17 and NMG-1), respectively. Sample NMG-1, collected from a crater lake, contains  $\text{Na}^+$ ,  $\text{Mg}^{2+}$ ,  $\text{Cl}^-$ , and  $\text{HCO}_3^{1-}$ . The well NMS-17 is 110 m in depth and it cuts down through alluvium, marl, tuff, and basalt. This succession forms a confined aquifer condition. The thickness of the aquiclude (marl) is about 50 m in the well NMS-17, and this aquiclude causes high-pressure effect on the aquifer system. Both wells NMG-1 and NMS-17 have high  $\text{SiO}_2$  content

(~76 ppm; Erisen et al. 1996). High salinity and  $P_{\text{CO}_2}$  (close to 1 bar) and high temperature (65°C) at the wellhead of NMS-17 and NMG-1 (44°C) indicate and existence of a subsurface geothermal reservoir. Figure 3 suggests that the geothermal gradient in the Misli basin ranges from the normal value (33°C/km) to three times higher values.

The thermal waters (NMS-11, NMS-17, and NMG-1) contain Na, Ca  $\text{HCO}_3$ -Cl, while the shallow groundwaters mainly compose of  $\text{CaHCO}_3$  type, and the mixed waters (NMS-20, NMS-27, and NMS-28) consist of Ca, Na  $\text{HCO}_3$ -Cl. The higher contents of  $\text{Na}^+$ , B, and  $\text{Cl}^-$ ,  $\text{HCO}_3^-$  in the thermal waters are typical for the area. The major hydrochemical process in the thermal waters is ion exchange, between  $\text{Na}^+$  and  $\text{Ca}^{2+}$  and Na and  $\text{Mg}^{2+}$ . Solution of calcareous materials (mainly in lapilli materials) in geothermal systems leads to an increase in  $\text{Ca}^{2+}$ , and this process yields to a  $\text{NaHCO}_3$ -type groundwater. Bicarbonate water can also reflect an influence of  $\text{CO}_2$  change in fluids at lower temperatures by mixing of local groundwater.

The chemical composition of the waters is plotted on a Schoeller diagram to show major constituents of the

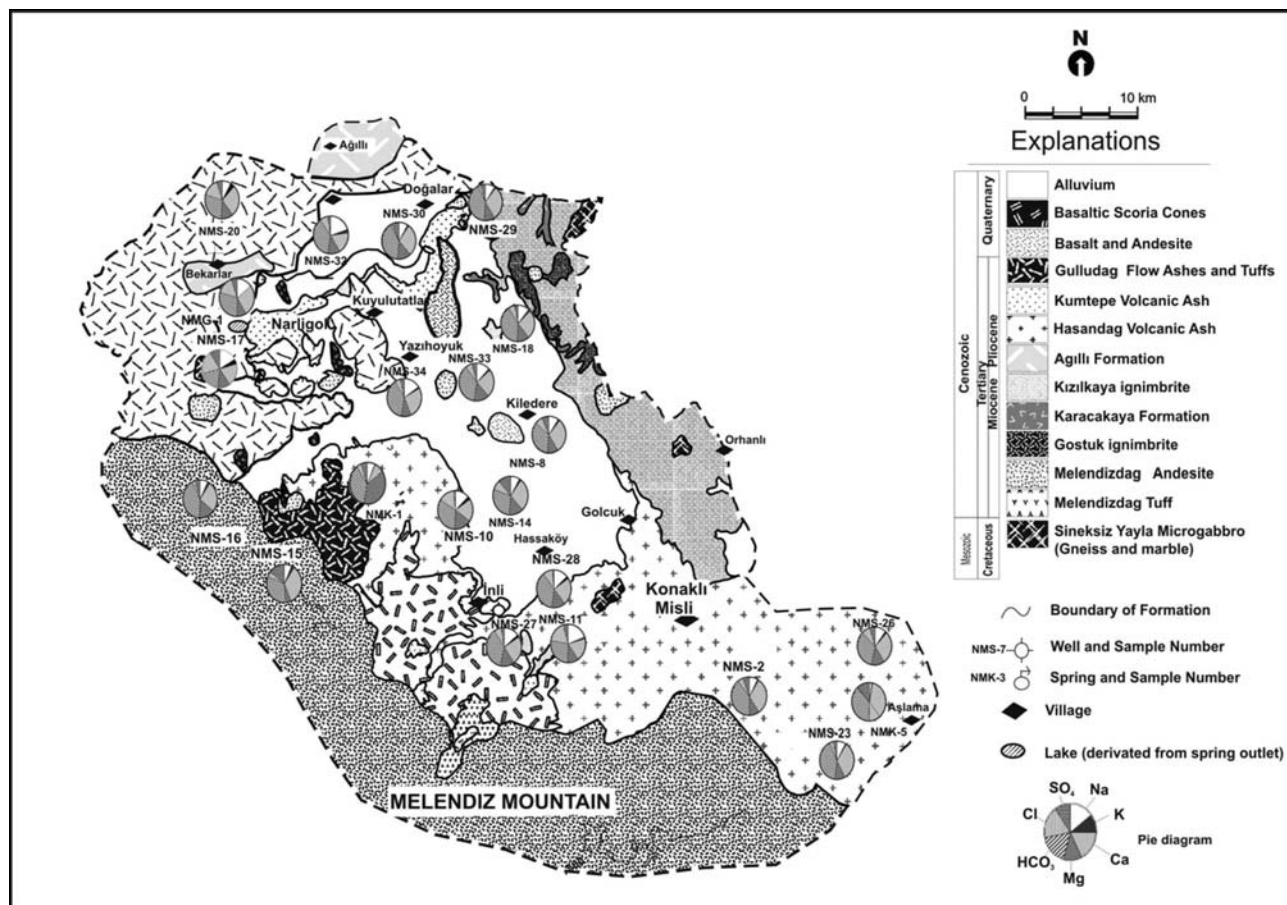


**Fig. 2** The distribution of major ions of the water samples with pie diagrams

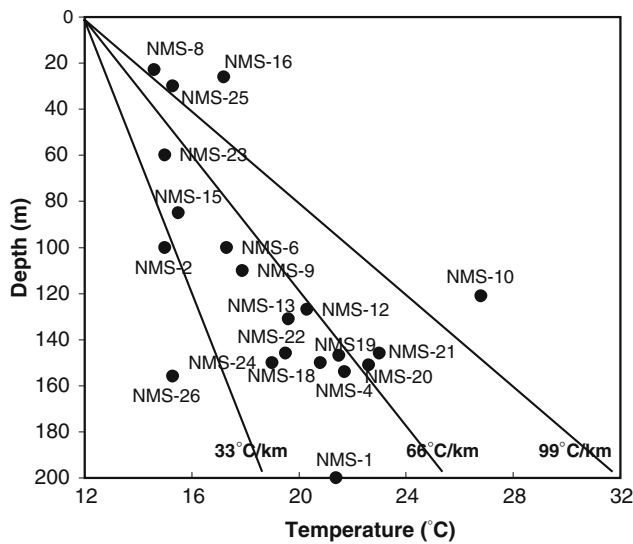


**Fig. 3** Temperature variations with depth

thermal, mixed, and cold waters in the study area. The thermal waters have higher concentration of  $\text{Na}^+$  and  $\text{HCO}_3\text{Cl}^-$  and relatively low  $\text{Ca}^{2+}$  and  $\text{Mg}^{2+}$  (Fig. 4a). The cold groundwaters contain higher  $\text{Ca}^{2+}$  and  $\text{Mg}^{2+}$  and have almost the same  $\text{HCO}_3^-$  content as the thermal waters, with the exception of shallow ones (Fig. 4b).

Boron and Cl relationship of water samples is given in Fig. 5. In Fig. 5, two end members—NMK-1 (representative of cold groundwater) and NMG-1 (representative of thermal water)—were considered to calculate mixing ratio between cold and thermal water using following equation:

$$C_M = C_Ax + C_B(1 - x) \tag{1}$$

where  $C_M$  denotes any of the conservative constituent (chloride values are taken into account for this study), subscripts A and B refer to the two end-members and  $x$  is the mass fraction of end-member A in mixture. The mixing ratios are listed in Table 1 and vary from 73.69% (for NMS-11) to 0.19% (for NMK-2).

The saturation index values with respect to the minerals calcite and dolomite were calculated by using the WATSPEC computer program (Wigley 1977). This program has been successfully used to predict mineral equilibrium states of various aqueous environments (Mutlu 1998; Mutlu and Güleç, 1998). The saturation indices of calcite and dolomite are plotted at the corresponding partial carbon dioxide pressure ( $P_{\text{CO}_2}$ ) of waters, which were also computed by the WATSPEC program (Fig. 6). Most waters are undersaturated with respect to both calcite and dolomite. Figure 6 also shows that SIs of the samples decrease with increasing  $P_{\text{CO}_2}$ .

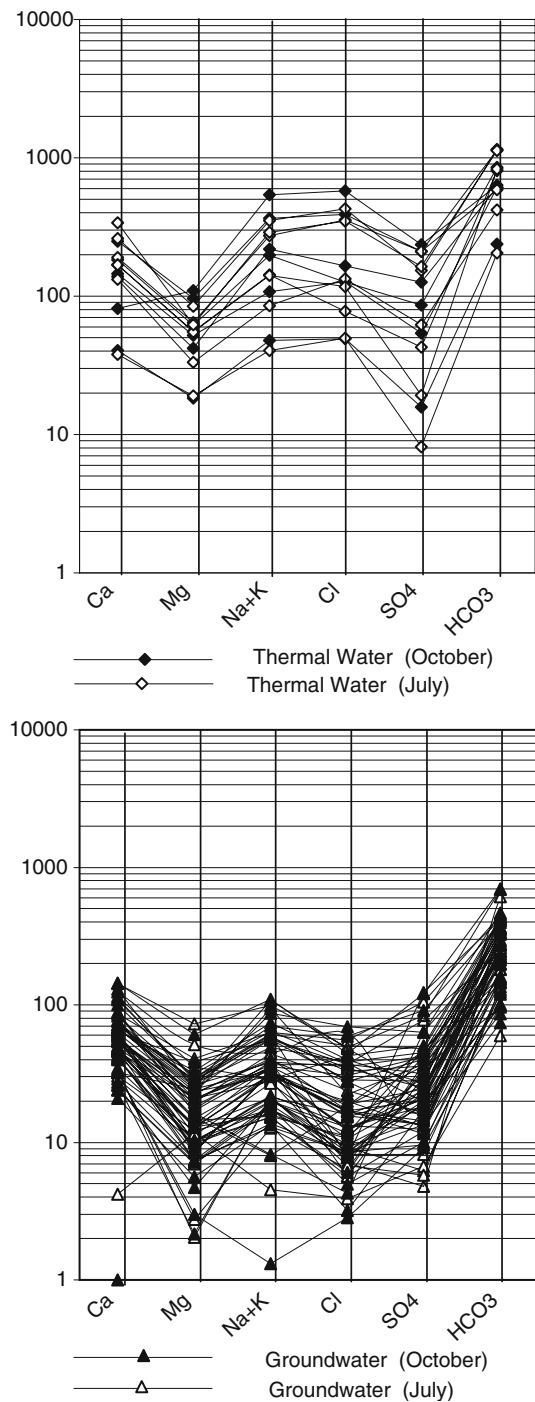


**Fig. 4 a** Schoeller diagram for thermal water. **b** Schoeller diagram for groundwater

The calculated carbon dioxide partial pressure values are extremely high, ranging from 0.93 to 6.16 atm, which are far above the atmospheric value ( $P_{\text{CO}_2} = 0.0003$  atm).  $P_{\text{CO}_2}$  versus  $\delta^{18}\text{O}$  diagram (Fig. 7) shows that the thermal and mixing waters are characterized with high partial pressure and enriched in  $\delta^{18}\text{O}$  values. Such high  $P_{\text{CO}_2}$  values might indicate the

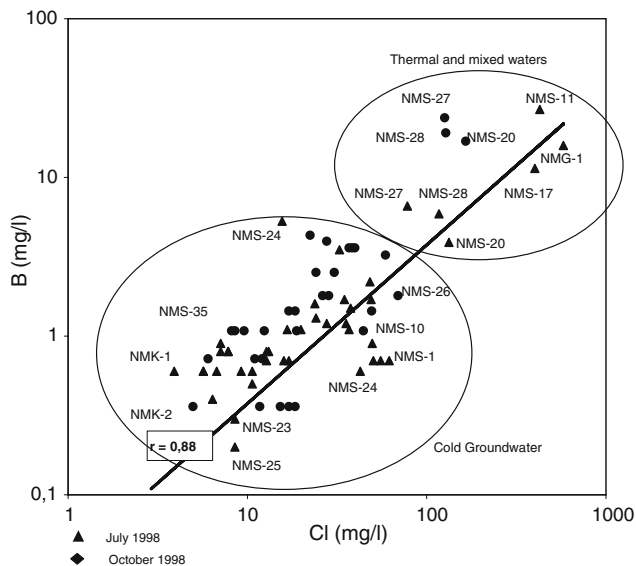


**Fig. 5** Chloride versus boron diagram

different subsurface physical and chemical processes. The thermal fluids would be over-saturated with respect to carbonate minerals at depth without the cold-water intrusion. As the thermal fluid upwards, it is mixed with cold groundwater of calcium-bicarbonate type at shallow depths. While thermal water ascends towards surface, the decrease in pressure permits the entry of fresh groundwater into the system. The temperature of the fluid decreases after degassing. Thus, it leads to an increase in calcium carbonate solubility. As a result of this dilution, thermal water becomes under-saturated with respect to calcium carbonate.

A further evaluation of the cation–anion distribution is made on ternary diagrams (Fig. 8a, b; Gignenbach 1988). Figure 8a shows the relative concentrations of  $\text{Cl-SO}_4\text{-HCO}_3$  of waters. All of the waters plot on the  $\text{HCO}_3$ -rich area; however, NMS-17 and NMG-1 relatively shifted to chloride-rich area. The relative Ca, Mg, Na + K concentrations of waters are shown on Fig. 8b. Most of the waters plot on the Ca area with the exceptions of samples of thermal and mixed waters (NMS-11, NMS-17, NMS-20, NMS-32, NMS-27, NMS-28, and NMG-1) and NMK-1 (cold groundwater).

Correlation of major ions with chloride are denoted on Fig. 9. The correlation coefficient of Cl with Na and Mg are about 0.96 and 0.84, respectively. Similarly, Cl and  $\text{SO}_4$  shows a close correlation ( $r = 0.86$ ). The  $\text{Ca}^{2+}/\text{Mg}^{2+}$  ratios of the waters, on the other hand, show a rather wide range and general proportion increase in dry period (October 1998). This may indicate that during the wet period,  $\text{CO}_2$  loss cause calcite precipitation mostly at shallow depths.  $\text{HCO}_3^-/\text{Cl}^-$  ratio of

thermal and mixed waters is below 2, which reflects deep Cl-rich influences by the thermal waters (Table 1).

Continuous pumping from shallow aquifer causes water quality degradation due to the vertical thermal water intrusion. Therefore, general trend in groundwater level decrease escalates year by year depending on heavy pumping. This spatial drawdown was measured between 1.5 and 3.5 m in 1996. This over-pumping increases the movement of high-mineralized water into the freshwater at shallow aquifer. For instance, EC values have increased from 2,980  $\mu\text{mho}/\text{cm}$  in 1993 to 3,596  $\mu\text{mho}/\text{cm}$  in 1998 for NMS-11, from 1,298  $\mu\text{mho}/\text{cm}$  in 1993 to 1,710  $\mu\text{mho}/\text{cm}$  in 1998 for NMS-20, from 1,535  $\mu\text{mho}/\text{cm}$  in 1993 to 2,020  $\mu\text{mho}/\text{cm}$  in 1998 for NMS-27, and from 1,682  $\mu\text{mho}/\text{cm}$  in 1993 to 1,726  $\mu\text{mho}/\text{cm}$  in 1998 for NMS-28 (Table 1). Thus, it is obviously seen that EC values have increased in time as a result of over-pumping, especially in the Inli region where thermal water widely discharged. Chloride and boron concentrations also increase. Boron increases in the deeper wells depending on the level of the first filter in consistence with thermal water influence (Fig. 10). On the other hand, boron content of groundwater at shallow depth is actually low; however, its concentration increases with depth because of the mixing with thermal water, which has high boron content.

#### Isotope chemistry

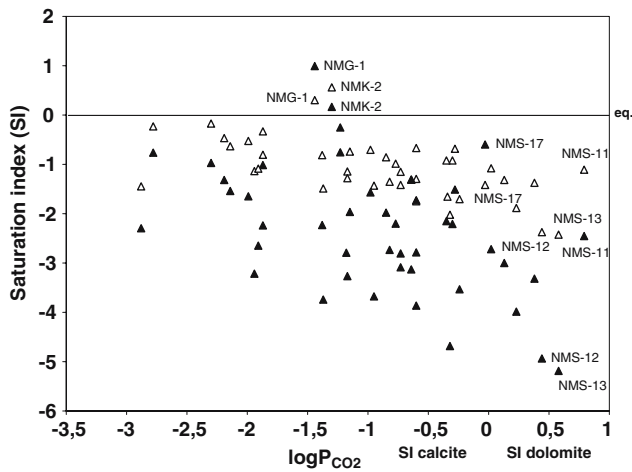
The results of oxygen and hydrogen isotope analyses of samples collected from the study area are given in Table 1 and are shown in the  $\delta^2\text{H}-\delta^{18}\text{O}$  plot (Fig. 11). Both the Global Meteoric Water Line (GMWL; Craig 1961) and the Eastern Mediterranean Water Line (EMWL; Gat and Carmi 1970) are shown as reference in Fig 11. All samples fall below the EMWL line while some of them are also below the GMWL line. The groundwater, therefore, appears to be recharged from both continental and Mediterranean precipitation. All the samples on the right of the GMWL are isotopically enriched due to either surface evaporation or mixing with thermal waters. Thermal and mixed waters show enriched values of  $\delta^{18}\text{O}$  and of  $\delta^2\text{H}$ . The  $\delta^{18}\text{O}$  and  $\delta^2\text{H}$  values of samples of October 1998 were slightly more enriched than those of July 1998 because of evaporation. Deviation from LMWL to the right of GMWL is typical for strong evaporative enrichment of non-thermal waters in heavier isotopes (Dansgaard 1964; Gat 1996). The fact that, samples NMS-17 and NMS-11 are characterized by the deviation from the GMWL in terms of  $\delta^{18}\text{O}$  and  $\delta^2\text{H}$  shows the enrichment due to the flushing by geothermal system. The slight oxygen-shift



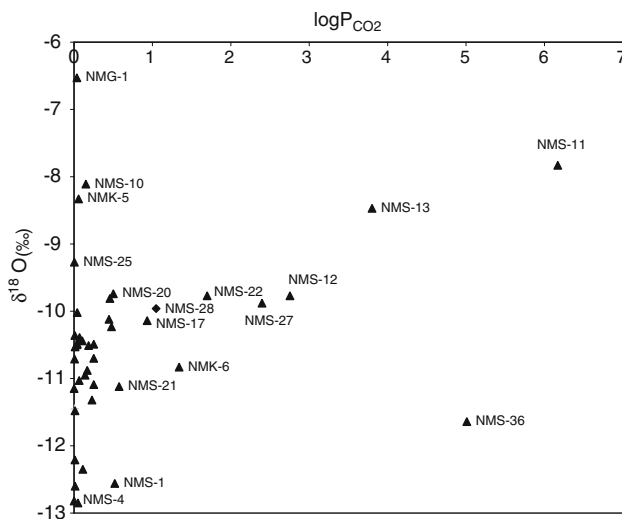


Table 1 continued

Sample no.	Sampling date	pH	EC at 25°C (µS/cm)	Cations (ppm)				Anions (ppm)				Total ions	%Na	Boron (mg/l)	Temperature (°C)	δ <sup>18</sup> O ‰	δD ‰	<sup>3</sup> H (TU)	Altitude (m)	Well depth (m)	Base level of well (m)	Static level from surface (m)	Static level as (m.a.s.l)	Q (yield) l/s	Ca/Mg (yield)	HCO <sub>3</sub> /Cl	Mixture content (%) of thermal water in ground water				
				Na	K	Ca	Mg	HCO <sub>3</sub>	Cl	SO <sub>4</sub>																					
NMS-28	20/07/1998	5.74	1.726	110.46	31.28	168.84	55.95	828.52	117.15	19.24	1331.44	25.8	5.9	-10.0	-73.2	3.4	1.305	176	1,129	5.5	1,299.5	63	1.83	4.11							
NMS-29	20/10/1998	6.19	1.456	92.24	15.64	146.33	52.66	611.61	127.80	54.35	1100.63	25	5.3	-9.4	-70.7	0.8	1.305	182.5	1182.5	76	1,289	30	3.26	2.78	21.6						
NMS-30	22/07/1998	6.21	4.93	20.98	5.87	61.51	11.46	257.23	10.65	21.65	389.34	18	0.6	-12.4	-86.1	2.6	1.365							3.26	14.03	1.2					
NMS-30	22/07/1998	7.04	3.83	15.22	5.87	46.83	13.17	199.19	7.81	25.01	313.09	15.6	0.8	-12.6	-84.8	2.3	1.365						2.16	14.82	2.5						
NMS-31	20/10/1998	6.83	4.61	0.23	7.82	56.28	15.36	211.41	18.46	46.66	356.21	16	0.1	-12.3	-81.9	2.0	1.418						2.22	6.65							
NMS-31	22/07/1998	6.1	6.51	24.90	13.29	71.56	26.45	369.04	7.10	4.81	517.16	15.1	0.9	-11.3	-83.4	2.2	1.325						1.64	30.20							
NMS-32	20/10/1998	6.26	4.04	24.67	16.03	55.88	23.16	327.50	17.04	11.54	475.82	17.4	0.1	-12.3	-83.6	1.3	1.325						1.46	11.17							
NMS-32	22/07/1998	6.24	9.79	86.48	21.51	68.54	25.84	432.59	48.28	23.57	706.80	38.1	2.2	-12.6	-88.3	4.6	1.280						1.67	11.30							
NMS-33	20/10/1998	6.5	7.95	74.95	19.55	62.71	22.80	435.03	22.37	37.04	674.44	37.2	1.2	-12.0	-83.4	4.5	1.280						1.67	11.30							
NMS-33	22/07/1998	5.77	7.91	45.66	13.29	75.78	27.43	363.55	32.66	36.08	594.44	23.7	3.5	-9.8	-76.9	2.6	1.296						1.68	6.47							
NMS-34	22/07/1998	6.17	8.10	46.58	13.29	71.76	29.01	358.05	27.69	40.40	586.78	24.3	1.1	-10.1	-73.8	2.9	1.296						1.50	7.51							
NMS-34	22/07/1998	6.47	4.27	27.67	5.87	41.41	8.53	180.25	15.62	13.47	292.81	29.2	5.3	-10.5	-70.4	3.3	1.330						2.94	6.70							
NMS-35	22/07/1998	7	2.99	16.14	1.17	30.55	12.31	124.64	9.23	6.25	200.31	21.5	0.6	-11.5	-82.3	2.5	1.305						1.50	7.85							
NMS-35	20/10/1998	7.12	2.53	17.76	1.17	27.54	7.56	129.53	8.17	8.18	199.90	27.6	0.3	-10.4	-75.5	2.8	1.305						2.21	9.22							
NMS-36	14/10/1998	8.2	2.30	16.14	5.08	26.53	2.19	74.54	8.52	13.47	146.48	30	0.6	-10.4	-77.4	0.2	1.382						7.33	5.08							
NMK-1	14/07/1998	7.66	1.26	4.15	0.39	4.22	11.82	59.88	3.91	6.73	91.10	13.1	0.6	-12.8	-83.9	11.2	1.598						0.22	8.91							
NMK-2	15/07/1998	7.47	2.62	14.53	7.04	33.97	2.07	135.64	6.75	5.77	205.77	0.24	0.6	-12.9	-84.2	1.6	1.472						9.94	11.68							
NMK-3	14/10/1998	8.01	2.18	8.76	9.38	24.12	7.31	119.76	4.97	10.10	184.41	16.1	0.1	-11.0	-70.1	3.7	1.195						2.87	9.00							
NMK-3	16/07/1998	6.45	4.53	15.68	4.30	49.65	10.48	197.96	12.78	18.28	309.13	16.5	0.8	-12.2	-81.8	1.8	1.472						2.00	14.00							
NMK-4	16/07/1998	6.54	8.44	51.19	13.29	65.73	32.18	413.65	37.63	19.72	633.39	26.2	1.5	-9.7	-73.0	3.7	1.195						2.51	10.45							
NMK-4	15/10/1998	7.01	8.59	57.65	16.42	65.53	33.64	459.47	39.76	26.94	699.41	27.2	1	-10.4	-72.2	0.4	1.184						1.24	6.39							
NMK-5	17/07/1998	6.81	10.15	51.65	11.73	86.83	41.45	449.70	55.38	104.86	801.60	20.2	0.7	-8.3	-64.8	13.1	1.402						2.27	4.72							
NMK-5	13/10/1998	7.86	9.93	55.34	14.86	109.34	29.74	397.15	58.93	91.39	756.76	22.5	0.9	-11.1	-75.3	0.3	1.184						1.18	6.71							
NMK-6	15/10/1998	7.01	1.550	56.50	43.01	143.72	73.63	694.10	48.99	84.18	1144.11	14.6	1.7	-11.3	-70.5	13.0	1.402						2.23	3.92							
NMK-6	14/10/1998	6.02	1.474	51.89	58.65	144.72	61.80	700.21	44.38	120.73	1182.37	14	0.3	-10.8	-83.3	4.3	1.279						1.42	9.17							
NMG-1	1990	6		210.54	26.20	128.64	24.38	733.20	255.60	1503.61	50.1	9.6	44	-9.6	-74.1	4.0	1.279						3.20	1.66							
NMG-1	16/07/1998	6.70	3.082	212.15	78.20	341.70	63.39	1134.02	347.90	163.54	2340.90	27.9	10.6	-6.5	-36.7	3.7	1.362						3.27	1.89							
NMG-2	15/10/1998	7.25	3.438	368.96	172.04	82.01	111.42	636.66	578.65	235.21	2184.95	47.5	15.9	-10.9	-80.7	2.0	1.155						0.45	0.64							
NMG-2	16/07/1998	6.28	6.47	35.97	10.95	58.89	20.60	306.72	24.14	16.35	473.63	24.1	1.3	-10.9	-80.7	2.0	1.155						1.73	7.38							
NMG-2	15/10/1998	7.37	6.58	44.28	11.73	64.32	39.01	414.26	28.40	27.90	629.89	27	0.5	-7.9	-70.0	2.0	1.155						1.00	8.48							



**Fig. 6** Saturation indices of calcite and dolomite as a function of  $P_{CO_2}$



**Fig. 7**  $\log P_{CO_2}$ – $\delta^{18}O$  diagram

of NMS-17 seems that the system has relatively shorter circulation than NMS-11, because NMS-17 has lower  $\delta^{18}O$  and  $\delta^2H$  values which indicate that hot water quickly moves upward to the surface. Thus, it could be inferred that permeability plays a more important role in NMS-17 than NMS-11 due to the fracture system it has. Similarly, the TDS and EC values are higher in NMS-11 than NMS-17, and tritium values of NMS-11 is lower than NMS-17 which supports the aforementioned situation. This relation indicates that water–rock interaction is dominant in NMS-11. NMG-1 exhibits a hydrogen shift (Fig. 11) possibly by exchange with  $H_2S$ , which might be attributed to isotopic exchange with  $H_2S$  content of the thermal water (Balderer 1999; Browne 1978). Accordingly,  $H_2S$  odor was felt near the bubbling pool NMG-1).

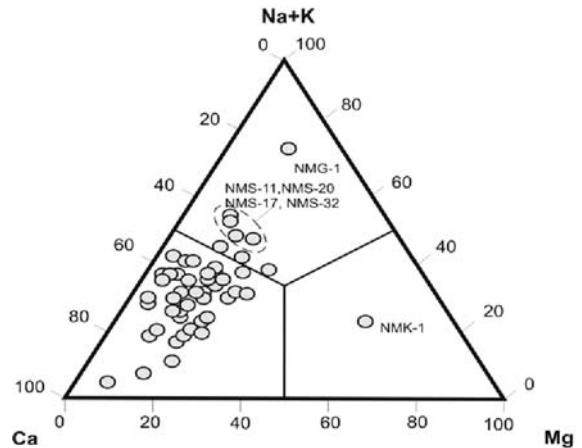
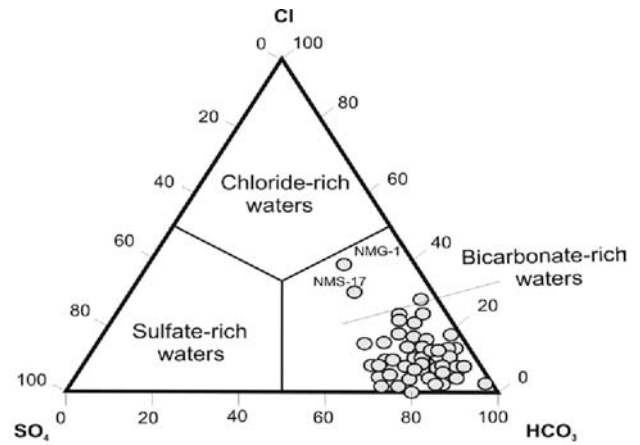


**Fig. 8 a and b.** Ternary Giggenbach (1988) diagrams: **a** Cl– $SO_4$ – $HCO_3$ , **b** (Na + K)–Ca–Mg

In low-temperature geothermal systems, oxygen shift is the main phenomenon in determining the isotopic composition of geothermal systems because the exchange reaction of oxygen isotope between water and mineral has very low rates. Thus, equilibrium will generally not be reached unless water has a long residence time in the reservoir (Nutti 1991). Thermal waters have the highest relative dissolved  $HCO_3$  content (Table 1). The depleted  $\delta^{18}O$  values of NMS-1, NMS-29, NMS-30, NMS-31, NMS-32, NMK-1, and NMK-2 indicate that groundwater is fed from higher altitudes (Fig. 11). Isotope analyses results of July 1998 of NMS-10, NMS-13, and NMK-5 were ignored because those waters were affected by evaporation after sampling. Figure 12 shows the relationship between low-chloride shallow groundwater and high-chloride thermal and mixed waters. The low-chloride waters with depleted oxygen-18 values are recharged from higher altitudes which represent short circulation of groundwater. The high-chloride with relatively enriched oxygen-18 values

**Fig. 9** Chloride versus ion concentration diagrams

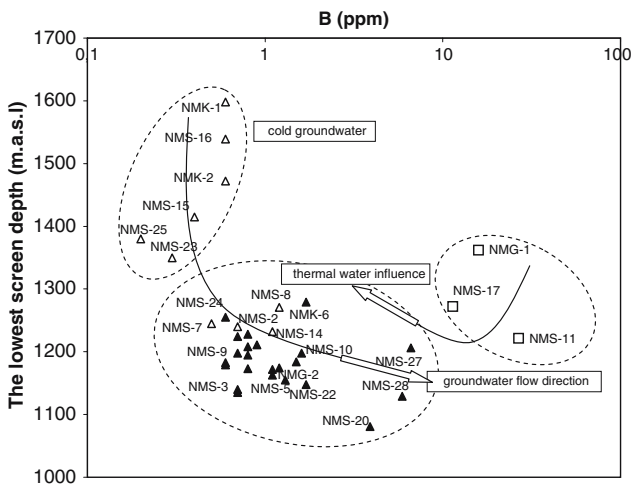
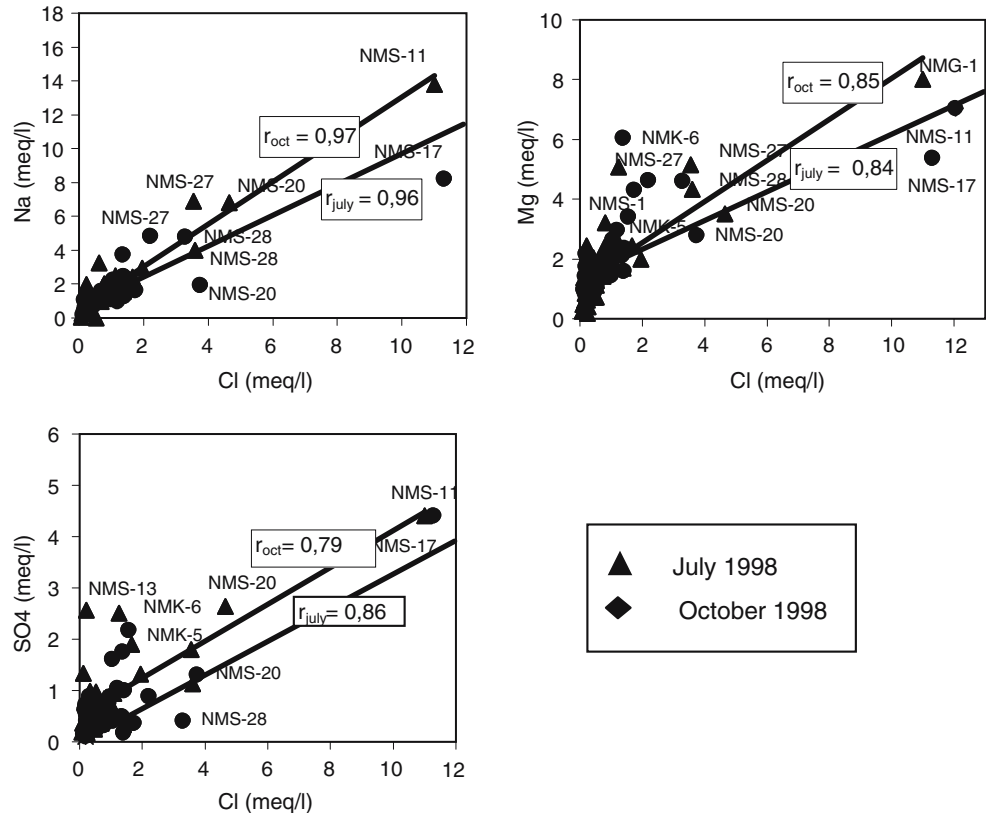


**Fig. 10** Boron variations with depth, showing boron increases by depth: open triangle cold waters, filled triangle mixing waters, open square thermal waters

refer to the thermal and mixed waters having long residence time in the aquifer system.

On the basis of the tritium versus depth plot (Fig. 13), the limit between high-<sup>3</sup>H waters and low-<sup>3</sup>H waters can be actually placed at depth close to 100 m, and an average tritium activity of  $1.6 \pm 1.2$  TU can be computed for the 44 low-<sup>3</sup>H water samples coming from the wells

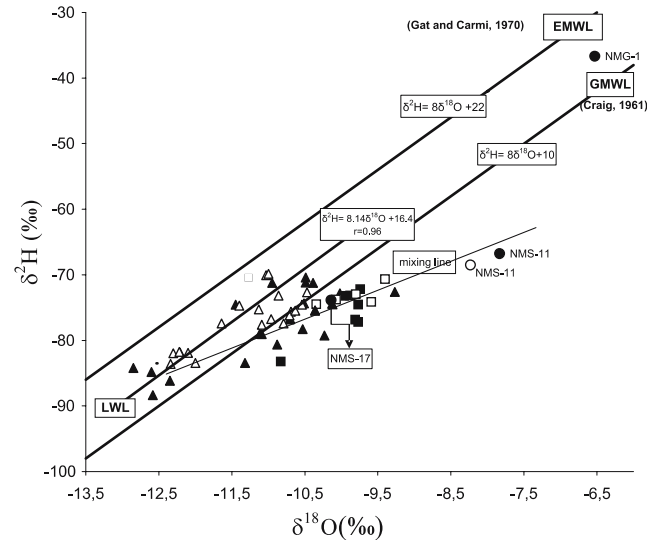


**Fig. 11**  $\delta^2\text{H}$  versus  $\delta^{18}\text{O}$  diagram of waters, showing isotopic differentiation related to thermal water effect. EMWL Eastern Mediterranean Water Line, LWL Local Water Line, GMWL Global Meteoric Water Line. Filled triangle July 1998 (groundwater), filled square July 1998 (mixing water), filled circle July 1998 (thermal water), open triangle October 1998 (groundwater), filled square October 1998 (mixing water), open circle October 1998 (thermal water)

deeper than 100 m. This small tritium activity implies both having a high residence time of ground water and an aquifer that recharged by pre-1963 precipitation.

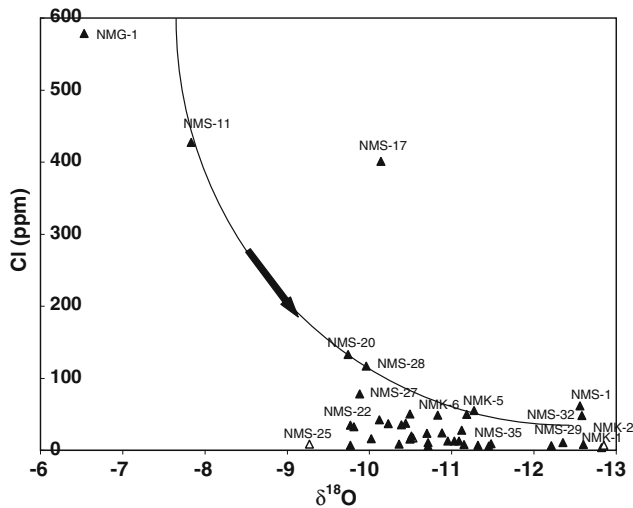


**Fig. 12** Chloride versus  $\delta^{18}\text{O}$  values showing the clustering of groundwater in the Misli Basin

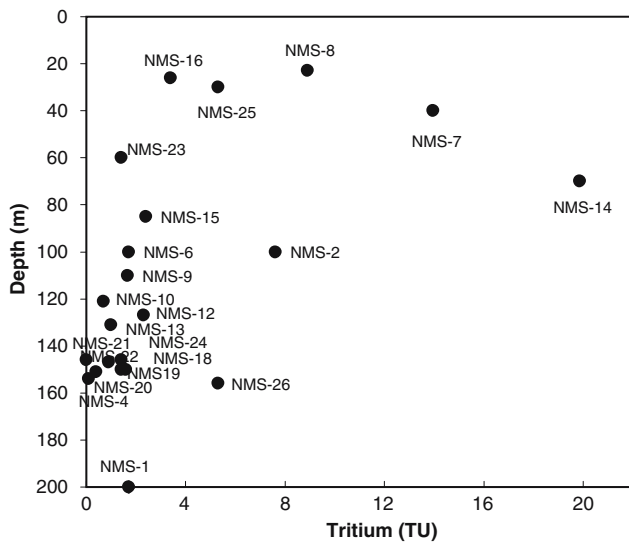


**Fig. 13** Tritium variations of the water with the depth

**Conclusions**

1. The shallow groundwater in the Misli Basin is represented by Ca, Mg  $\text{HCO}_3$ -type waters. Most thermal waters in the basin are generally enriched in  $\text{Na}^+ - \text{Cl}^- - \text{HCO}_3^-$ , while the groundwater has been linearly enriched by the  $\text{Na}^+$  and  $\text{Cl}^-$  contents as a result of the influence of thermal waters. The high Cl concentration of groundwater is sourced from the deep circulation of water having a long residence time in the reservoir.
2. No water in the Misli Basin reaches to water-rock chemical equilibrium. All waters are plotted

3. Stable isotope composition of waters suggests that thermal waters in the Misli basin are of meteoric origin although slightly enriched in  $\delta^{18}\text{O}$ .
4. Highly permeable alluvium existing in the middle of the Misli basin permits rapid and deep infiltration of recent meteoric water into the deeper aquifer system. This situation is observed in samples collected from the shallow wells with high tritium values.
5. The tritium value of the deep circulating groundwater is rather low, and values range from 0 to 2.7 TU. The average tritium activity of  $1.6 \pm 1.2$  TU can be computed for the 44 low  $^3\text{H}$  water samples coming from wells whose depths are deeper than 100 m. This small tritium activity indicates a high residence time and that the aquifer is mostly recharged from pre-1963 precipitation. The tritium values of the deep circulation at NW of the area are enriched with the contribution of relatively recent waters circulating from the northern area and reach up to 4.6 TU with depleted heavy isotope contents (in NMS-29, NMS-30, NMS-31, NMS-32).
6. The chemical and isotopic composition of the thermal and cold waters seem to be affected by the over-exploitation of the reservoir, and it is rather difficult to distinguish all types of waters with respect to chemical composition. However, the thermal waters can be distinguished from the meteoric waters with their enriched values with respect to  $\delta^{18}\text{O}$  and  $\delta^2\text{H}$ .
7. The local geothermal gradient ranges from the normal value ( $33^\circ\text{C}/\text{km}$ ) to three times higher. The origin of geothermal resource is the meteoric waters that can be somehow infiltrated into subterranean environment, and after being heated by the results of past volcanic activities, it moves upward to the surface along a fault zone as a thermal water.

To conclude, a further lowering of the groundwater table would force the mobilization of thermal waters with a high salinity. As a result of this influence, certain chemical components such as Na, B, and Cl, would increase in the shallow groundwater in accordance with over-pumping. Thus, groundwater quality would be deteriorated due to man-made activity. The relative increase in sodium with respect to calcium would lead to a modification of soil structure and hydrological properties marked by a significant

degradation of permeability, porosity, and agricultural properties.

The lowering of the groundwater level would accelerate the thermal water intrusion at deeper parts of aquifer and deteriorate the water quality depending on the increase in groundwater demand. The groundwater exploitation and management should be carried out carefully by taking groundwater level-quality control measurements into consideration.

**Acknowledgement** This study was performed by the General Directorate of State Hydraulic Works of Turkey (DSİ) as a research project. The author thanks DSİ, mainly Mr. Erol Onhon for his valuable contribution to the manuscript. Special thanks to Mr. Mesut Sayın who did isotope analyses in the laboratory of DSİ, and to Mrs. Nihal Basaran and to Mr. Ugur Sural for their efforts to carry out the project. The author is also indebted to Dr. Halim Mutlu, Dr. Tolga Yalcin, and Didem Ugurluoglu for helping and editing of the manuscript. The author would like to send his deep gratefulness to Prof. Luigi Marini and Prof. Stuart F. Simmons for their efficient help and re-evaluation of the paper.

## References

- Balderer W (1999) Application of isotope techniques in hydrogeology. Department of Geological Engineering, Faculty of Mining, Istanbul Technical University, Istanbul
- Browne PRL (1978) Hydrothermal alteration in active geothermal fields. *Annu Rev Earth Planet Sci* 6:229–250
- Bursalı S, Ertan I, Yalçın H, Günay G, Önhon E (1975) Determination of groundwater characteristics in the Niğde-Misli Plain by means of isotopes. IAEA-State Hydraulic Works, Ankara
- Craig H (1961) Isotopic variations in meteoric waters. *Science* 133:1702–1703
- Dansgaard W (1964) Stable isotopes in precipitation. *Tellus* 16:436–446
- Erisen B, Akkus I, Uygur N, Kocak A (1996) The Geothermal Inventory of Turkey (in Turkish). General Directorate of Mineral Research and Exploration (MTA), MTA Publications, Ankara, pp 370–376
- Gat JR, Carmi L (1970) Evolution of the isotopic composition of atmospheric waters in the Mediterranean Sea area. *J Geophys Res* 75:3039–3048
- Gat JR (1996) Oxygen and hydrogen isotopes in hydrologic cycle. *Annu Rev Earth Planet Sci* 24:225–262
- Giggenbach WF (1988) Geothermal solute equilibria. Derivation of Na–K–Ca–Mg geothermometers. *Geochim Cosmochim Acta* 52:2749–2765
- Gulenbay A (1971) The hydrogeological investigation of Niğde-Misli Plain. In: Planning stage. State Hydraulic Works (DSİ), Ankara
- Mutlu H (1998) Chemical geothermometry and fluid-mineral equilibria for the Ömer-Gecek thermal waters, Afyon Area, Turkey. *J Volcanol Geotherm Res* 80(3–4):303–321
- Mutlu H, Güleç N (1998) Hydrogeochemical outline of thermal waters and geothermometry applications in Anatolia, Turkey. *J Volcanol Geotherm Res* 85(1–4):495–515
- Nuti S (1991) Isotope techniques in geothermal studies. In: D'Amore (coordinator), Applications of geochemistry in geothermal reservoir development. UNITAR/UNDP publication, Rome, pp 215–251
- Verhagen B Th, Geyh M A, Fröhlich K, With K (1991) Isotope hydrological methods for the quantitative evaluation of groundwater resources in arid and semi-arid areas. Research Reports of the Federal Ministry for economic cooperation of the Federal Republic of Germany, Bonn, pp 7–122
- Wigley TML (1977) WATSPEC: a computer program for determining the equilibrium speciation of aqueous solutions. *British Geomorphology Research Group Technical Bulletin*, pp 20–48
- Yurdagül M (1998) Revisional hydrogeological study report of Niğde-Misli Basin (in Turkish). State Hydraulic Works (DSİ), Ankara